Molecular Crystals and Liquid Crystals Science and Technology. Section A. Molecular Crystals and Liquid Crystals

Publication details, including instructions for authors and subscription information:
http://www.tandfonline.com/loi/gmcl19

Two Interesting Features in the Infrared and Raman Spectra of the 12K Organic Superconductor κ-$(ET)_2Cu[N(CN)_2]Br$

J. E. Eldridge [a], Y. Xie [a], H. H. Wang [b], J. M. Williams [b], A. M. Kini [b] & J. A. Schlueter [b]

[a] Department of Physics, University of British Columbia, Vancouver, B.C., V6T 1Z1, Canada

[b] Chemistry and Materials Science Division, Argonne National Laboratory, Argonne, IL, 60439, USA

Version of record first published: 24 Sep 2006.

To cite this article: J. E. Eldridge , Y. Xie , H. H. Wang , J. M. Williams , A. M. Kini & J. A. Schlueter (1996): Two Interesting Features in the Infrared and Raman Spectra of the 12K Organic Superconductor κ-$(ET)_2Cu[N(CN)_2]Br$, Molecular Crystals and Liquid Crystals Science and Technology. Section A. Molecular Crystals and Liquid Crystals, 284:1, 97-106

To link to this article: http://dx.doi.org/10.1080/10587259608037914

Mol. Cryst. Liq. Cryst., 1996, Vol. 284, pp. 97–106
Reprints available directly from the publisher
Photocopying permitted by license only

TWO INTERESTING FEATURES IN THE INFRARED AND RAMAN SPECTRA OF THE 12K ORGANIC SUPERCONDUCTOR $\varkappa$-$(ET)_2Cu[N(CN)_2]Br$.

J. E. ELDRIDGE AND Y. XIE
Department of Physics, University of British Columbia, Vancouver, B.C., V6T 1Z1, Canada.

H. H. WANG, J. M. WILLIAMS, A. M. KINI, AND J. A. SCHLUETER
Chemistry and Materials Science Division, Argonne National Laboratory, Argonne, IL 60439, USA

Abstract Two of the larger features in the infrared conductivity spectra of $\varkappa$-$(ET)_2Cu[N(CN)_2]Br$ are analysed and one is reassigned with the aid of infrared and Raman spectra of isotopically-substituted compounds.

Figure 1 shows the infrared conductivity of ET copper dicyanimide bromide at various temperatures[1]. One can see that as the material is cooled the far-infrared intraband electronic conductivity, due to the free carriers, grows at the expense of the mid-infrared interband conductivity. This paper, however, is not concerned with this aspect of the spectrum but rather with two of the larger vibrational features.

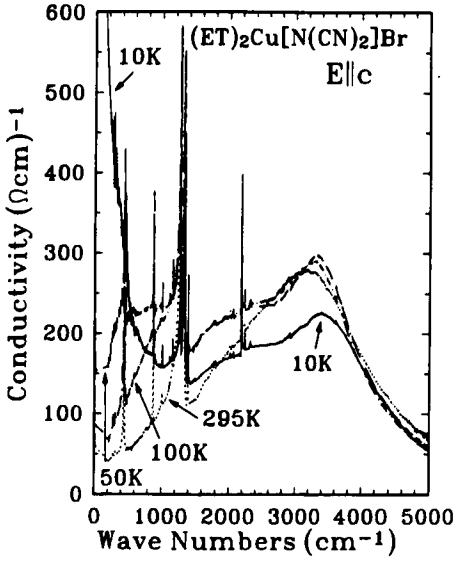

FIGURE 1 The infrared conductivity as a function of temperature.

The first is the large resonance near 1300 cm^{-1}, correctly assigned to $\nu_3(A_g)$ but which we will show has changed its nature in this solid, and the second is the sharp line near 880 cm^{-1}, which we will show has consistently been misassigned.

THE 1300 cm^{-1} RESONANCE

This large resonance could have been either $\nu_2(A_g)$ or $\nu_3(A_g)$, both of which are shown in Fig. 2 and which involve the vibration of the same two carbon pairs, but with a 180° phase difference in the case of $\nu_2(A_g)$. The reason that these totally-symmetric Raman active vibrations are also infrared active, is the well-known vibronic mechanism whereby charge is transferred between molecules, which are arranged in dimer pairs, as they vibrate out of phase with each other. The size of the molecule depends on the amount of charge it has and therefore the charge will oscillate between the two molecules as they alternately expand and contract. This produces an infrared activity for radiation with the electric field vector polarized *perpendicular* to the molecular plane.

We have recently published a comprehensive analysis of all of the in-plane vibrations of the ET molecule[2]. There are 72 fundamental intramolecular ("internal") normal modes, distributed among the D_{2h} (planar) symmetry species as follows:

$$\Gamma(D_{2h}) = 12A_g + 6B_{1g} + 7B_{2g} + 11B_{3g} + 7A_u + 11B_{1u} + 11B_{2u} + 7B_{3u} \quad (1)$$

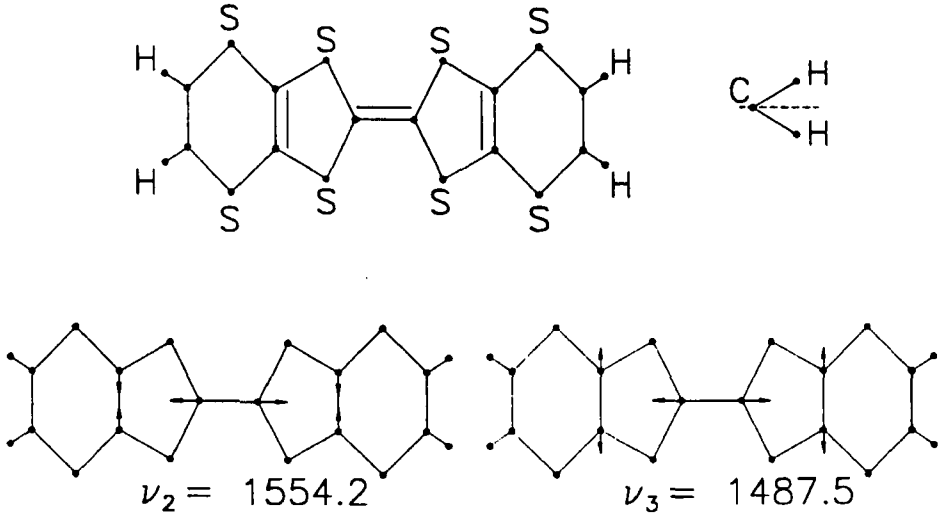

FIGURE 2 The ET molecule and the $\nu_2(A_g)$ and $\nu_3(A_g)$ normal vibrations.

The frequencies of these modes change when the mass of the atoms involved changes (the *isotope* effect) or when the charge on the molecule changes (the *ionicity* effect) or when the vibration is coupled to the charge transfer (the *electron-phonon* effect). Figure 3 shows the isotopic analogs we used in the analysis[2] of ET and Table 1 shows the agreement we obtained between the calculated and observed frequencies and isotopic frequency shifts for the first four A_g modes. One can see that with ^{13}C at only the central pair sites, both $\nu_2(A_g)$ and $\nu_3(A_g)$ give 30 cm^{-1} shifts while with ^{13}C at the inner six sites both modes have twice the shift or approximately 60 cm^{-1}. This shows that in ET both of these modes involve the central carbon atom pair and the inner-ring carbon atom pairs fairly equally.

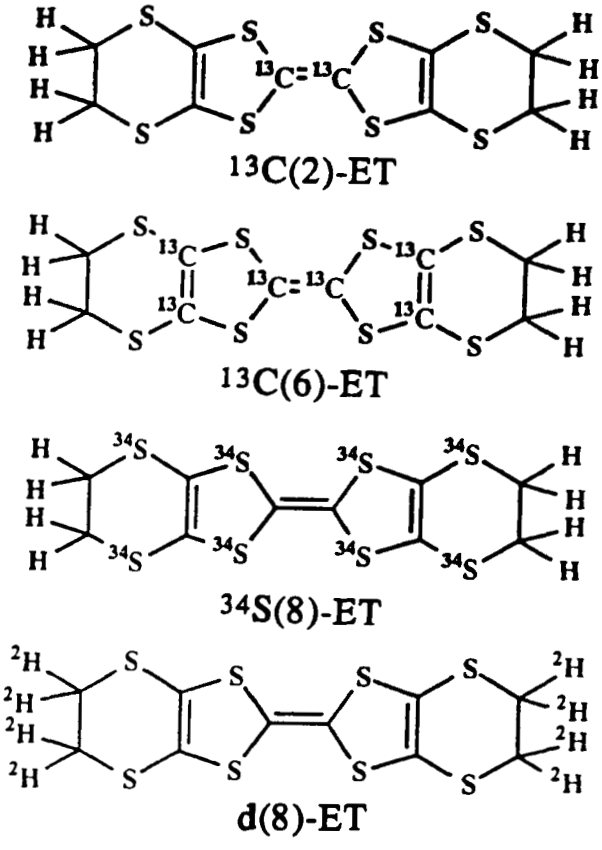

FIGURE 3 The four isotopic analogs of ET used in this study.

TABLE 1 Calculated and observed frequencies and isotopic frequency shifts of the first four totally-symmetric modes.

		$\nu_1(A_g)$	$\nu_2(A_g)$	$\nu_3(A_g)$	$\nu_4(A_g)$
ν	CALC.	2941	1554	1488	1413
cm^{-1}	OBS.	2920	1551	1493	1408
$\Delta\nu$	CALC.	0	-27	-33	-1
$^{13}C(2)$	OBS.	0	-29	-28	0
$\Delta\nu$	CALC.	0	-60	-58	-1
$^{13}C(6)$	OBS.	0	-65	-56	0
$\Delta\nu$	CALC.	0	0	-1	0
$^{34}S(8)$	OBS.	0	-2	0	0
$\Delta\nu$	CALC.	-788	0	0	-363
$^{2}H(8)$	OBS.	-773	0	+1	-292

Consider now $\nu_2(A_g)$. Table 2 lists both Raman and infrared data. In the Raman data are listed the ionicity shift in going from ET to $(ET)_2Cu[N(CN)_2]Br$ and then the 60 cm^{-1} shift, mentioned above, in the $^{13}C(6)$ compound. In the infrared spectra, however, after the electron-phonon shift, one sees that in the $^{13}C(2)$ compound *there is no 30 cm^{-1} negative shift* but rather a slightly positive one, whereas in the $^{13}C(6)$ compound the full 60 cm^{-1} shift is observed. This means that in the conducting solid $\nu_2(A_g)$ has changed its nature and *now involves only the inner-ring carbon pair* as drawn in Fig. 4. Figure 5 shows the spectra in question and the features due to $\nu_2(A_g)$ may be observed.

TABLE 2 Experimental infrared and Raman data for $\nu_2(A_g)$ in ET and $(ET)_2Cu[N(CN)_2]Br$. Frequencies and frequency shifts are listed and labelled.

$\nu_2(A_g)$

RAMAN

ET	^{13}C(2)-ET	^{13}C(6)-ET	$(ET)_2^+Cu[N(CN)_2]Br^-$	^{13}C(6)-x-$(ET)_2^+Cu[N(CN)_2]Br^-$
1551	1522 **(-29)**	1486 **(-65)**	1496 (-55)	1436 (-60)
	isotope	isotope	ionicity	isotope

INFRARED Ella

$(ET)_2^+Cu[N(CN)_2]Br^-$	^{13}C(2)-x-$(ET)_2^+Cu[N(CN)_2]Br^-$	^{13}C(6)-x-$(ET)_2^+Cu[N(CN)_2]Br^-$
1480 (-16)	1485 (+5)	1419 **(-61)**
1472 (-24)	1474 (+2)	1414 **(-58)**
electron-phonon	isotope	isotope

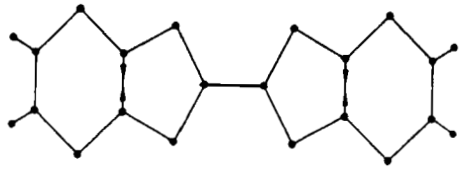

FIGURE 4 The atomic displacements in $\nu_2(A_g)$ in the conducting solid $(ET)_2Cu[N(CN)_2]Br$. Notice that only the inner-ring carbon atom pair is vibrating and not the central pair.

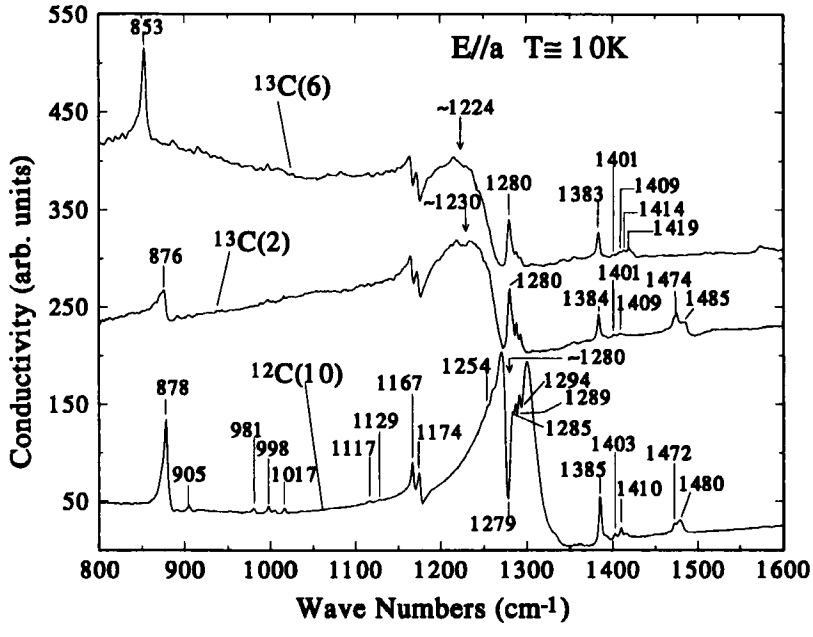

FIGURE 5 The 10K infrared conductivity for **Ella**, obtained from a Kramers-Kronig analysis of the reflectivity, of natural κ-$(ET)_2^+Cu[N(CN)_2]Br^-$, together with those of the two compounds with ^{13}C isotopic substitutions. Not all of the features in these latter spectra have been labelled. The ^{13}C spectra have been offset for clarity.

Similarly consider now $\nu_3(A_g)$. Table 3 lists the appropriate data. Comparing the infrared isotope shifts in this case one sees that for the $^{13}C(2)$ compound the observed 50 cm^{-1} shift is almost equal to the full 56 cm^{-1} shift seen in the $^{13}C(6)$ compound. This means that this mode has also changed its nature, presumably because of the very strong electron-phonon coupling, *and now consists of the vibration of only the central carbon pair* as drawn in Fig.6. The intense broad infrared feature due to $\nu_3(A_g)$ may also be seen in Fig.5 where it is complicated by the presence of the interacting sharp ν_5 (A_g) quartet with the strongest line near 1280 cm^{-1}. These data are being published in more detail elsewhere[3].

TABLE 3 Experimental infrared and Raman data for $\nu_3(A_g)$ in ET and $(ET)_2Cu[N(CN)_2]Br$. Frequencies and frequency shifts are listed and labelled.

ν_3 (A_g)

RAMAN

ET	^{13}C(2)-ET	^{13}C(6)-ET	$(ET)_2^+Cu[N(CN)_2]Br^-$	^{13}C(6)-$\varkappa$-$(ET)_2^+Cu[N(CN)_2]Br^-$
1494	1465 (-28)	1437 (-56)	1468 (-25)	1415 (-53)
	isotope	isotope	ionicity	isotope

INFRARED Ella

$(ET)_2^+Cu[N(CN)_2]Br^-$	^{13}C(2)-$\varkappa$-$(ET)_2^+Cu[N(CN)_2]Br^-$	^{13}C(6)-$\varkappa$-$(ET)_2^+Cu[N(CN)_2]Br^-$
~1280 (-188)	~1230 (-50)	~1224 (-56)
electron-phonon	isotope	isotope

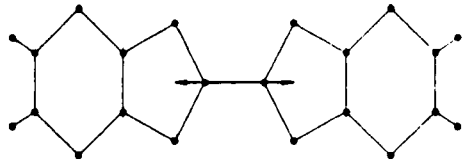

FIGURE 6 The atomic displacements in $\nu_3(A_g)$ in the conducting solid $(ET)_2Cu[N(CN)_2]Br$. Notice that only the central carbon atom pair is vibrating and not those in the inner ring.

THE 880 cm^{-1} SHARP RESONANCE

The 880 cm^{-1} resonance for **Ellc** (878 cm^{-1} for **Ella**) seen in Fig. 1 has been previously assigned to ν_7 (A_g) by several authors and to $\nu_{49}(B_{2u})$ by us before we had Raman data. In the Raman spectrum of ET, shown as the lower dashed curve in Fig.7 below, there is no strong or sharp feature at that wavenumber. In the $\varkappa$-$(ET)_2Cu[N(CN)_2]Br$ spectrum, on the other hand, shown as the solid curve in the same figure below, there now appear two new strong features, one at 889 cm^{-1} and the other at 827 cm^{-1}. This latter resonance at 827 cm^{-1} displays no $^{13}C(6)$ shift and so we have assigned it[3] to an out-of-plane C-H mode, $\nu_{22}(B_{1g})$, calculated[2] to occur at 835 cm^{-1}.

We are fairly sure, however, that the 889 cm^{-1} Raman feature is due to the same mode which is responsible for the 878 cm^{-1} infrared feature. Both of them display a 25 or 26 cm^{-1} isotope shift in the $^{13}C(6)$ compound as shown in the top part of Table 4 ("experimental"). What mode therefore can it be ? We have listed in the bottom part of Table 4 the calculated frequencies and isotope shifts of the modes which we consider to be the possibilities and now discuss them in order.

The first is ν_6 (A_g) which has the correct isotope shifts, but with a frequency of 983 cm^{-1} this would involve an ionicity shift of over 100 cm^{-1} in going from ET to

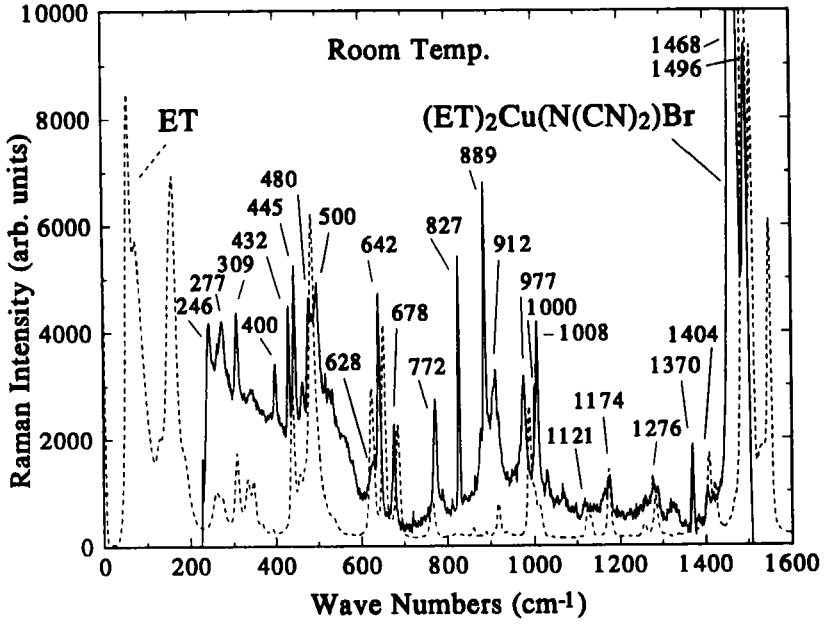

FIGURE 7 The room temperature Raman spectrum of $\varkappa$-$(ET)_2Cu[N(CN)_2]Br$, together with the room temperature Raman spectrum of neutral ET, taken from Ref. 2.

κ-$(ET)_2^+Cu[N(CN)_2]Br^-$, which is twice that observed for $\nu_3(A_g)$. The next, ν_7 (A_g), is not a serious candidate since it involves the hydrogen atoms, which the infrared data clearly dispute. The next two, $\nu_{48}(B_{2u})$ and $\nu_{49}(B_{2u})$ both have the correct frequency and isotope shifts, which is why we originally assigned the feature to $\nu_{49}(B_{2u})$ but there is no reason for these modes, which are infrared active, to be so strong in the Raman spectrum.

TABLE 4 Experimental frequencies and shifts of the "880 cm^{-1}" feature in κ-$(ET)_2^+Cu[N(CN)_2]Br^-$ together with the calculated frequencies and shifts of modes which have approximately the same frequency in neutral ET.

κ-$(ET)_2^+Cu[N(CN)_2]Br^-$

EXPERIMENTAL

	Natural	$^{13}C(2)$ -	$^{13}C(6)$ -	$^{34}S(8)$ -	$^{2}H(8)$
	ν	$\Delta\nu$	$\Delta\nu$	$\Delta\nu$	$\Delta\nu$
INFRARED Ella	878	-2	-25	-4	+7
RAMAN	889	-1[a]	-26	-3[a]	-8[a]

ET

CALCULATED

ν_6 (A_g)	983	-1	-32	-6	-6
ν_7 (A_g)	918	0	-1	-1	-188
$\nu_{48}(B_{2u})$	904	-7	-25	-7	-2
$\nu_{49}(B_{2u})$	890	-20	-27	-5	-2
$\nu_{60}(B_{3g})$	889	-2	-26	-6	-4

[a] very weak feature in neutral ET

Our best guess, therefore, is the last candidate, $\nu_{60}(B_{3g})$. It is normally Raman active, and is drawn below in Fig. 8. It involves the inner-ring carbon atom pairs. The lower part of Fig. 8 shows the molecular arrangement in a $\varkappa$-phase material, where the lines represent the *end* views of the molecules arranged in dimers with alternating orientation. The reason for the infrared activity of this mode may be as follows. If adjacent molecules in a dimer are oscillating out of phase in the $\nu_{60}(B_{3g})$ mode, then their orbital overlap is changing and in a $\varkappa$-phase material this may cause charge to transfer from one dimer to an adjacent dimer, producing the dipole needed for infrared activity. We have also assigned other infrared features to B_{3g} modes[3].

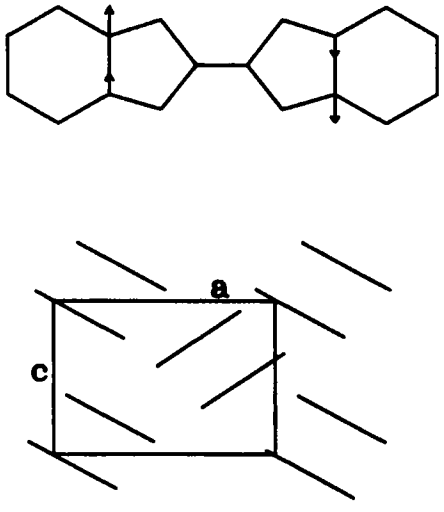

FIGURE 8 Top: An approximate representation of the $\nu_{60}(B_{3g})$ normal mode. Bottom: A sketch of the unit cell in the ac plane showing the end views of the molecular dimers (i.e. their long axes are normal to this ac plane).

REFERENCES

1. J. E. Eldridge, K. Kornelsen, H. H. Wang, J. M. Williams, A. V. Strieby Crouch and D. M. Watkins, Solid State Commun., 79, 583 (1991).
2. J. E. Eldridge, C. C. Homes, J. M. Williams, A. M. Kini, and H. H. Wang, Spectrochimica Acta, 51A, No. 6, 947 (1995).
3. J. E. Eldridge, Y. Xie, H. H. Wang, J. M. Williams, A. M. Kini, and J. A. Schlueter, Spectrochimica Acta, 52A, No. 1, (Jan. 1996).